Winglet Analysis for a Long-Endurance Cargo UAV

A Planar Parametric Aerodynamic Study via Vortex-Lattice Analysis

AEROSP 638 Final Project

April 24, 2026

Abstract

This study examines how winglets affect the aerodynamic performance of a long-endurance cargo unmanned aerial vehicle (UAV) at cruise. Rather than modeling winglets as a separate non-planar surface, which is numerically difficult at low fidelity, we adopt the Whitcomb principle that a winglet provides induced drag reduction primarily by extending the wing's effective span. A planar wing with a higher aspect ratio therefore represents a clean upper bound on the induced drag benefit that any winglet of comparable height could deliver. We use this equivalence as the framing for a parametric study performed with the OpenAeroStruct vortex-lattice code, sweeping aspect ratio, taper ratio, and tip washout for a 3500 kg, 19 m span cargo UAV cruising at 15,000 ft. Results show that a notional winglet of approximately 1.5 m equivalent height could improve cruise lift-to-drag ratio by up to 15 percent, while a more achievable 1 m vertical winglet corresponds to roughly 8 to 10 percent. We also find that taper ratio and tip washout both shape the spanwise lift distribution toward elliptical loading, with a taper of 0.3 to 0.5 combined with mild positive twist giving span efficiency very close to unity.

1 Introduction and Motivation

Long-endurance cargo UAVs spend most of their mission in steady cruise, and their range is governed almost entirely by lift-to-drag ratio. For a battery or fuel-based aircraft, the Breguet range equation shows that range scales linearly with L/D, so even a modest drag reduction translates directly into longer missions or larger payloads. At cruise lift coefficients typical of a high aspect ratio wing, induced drag is the largest single component of total drag, often accounting for 35 to 45 percent. Reducing induced drag is therefore one of the most important levers in the cruise design space.

The most common way to reduce induced drag at fixed wingspan is to add a winglet. The 1976 NASA study by Whitcomb [2] introduced the modern winglet concept and showed that a properly designed vertical surface at the wingtip can reduce induced drag by 5 to 10 percent. The mechanism is geometric. The trailing vortex pattern that produces induced drag depends on the spanwise distribution of bound circulation. By moving the strongest portion of the trailing vortex farther from the wing plane, a winglet effectively widens the wake and reduces the downwash felt by the wing. This is functionally similar to lengthening the span, but it accomplishes the same goal within a fixed wingtip-to-wingtip footprint, which matters when ground operations or hangar dimensions limit how wide the aircraft can be.

The objective of this project is to quantify the upper bound of winglet benefit for a representative cargo UAV, and to put that benefit in context with the other planform variables (taper and twist) that also shape the lift distribution. The aircraft modeled here is a notional 3500 kg cargo UAV with 1000 kg payload, designed for a 3000 km cruise at 15,000 ft. The wing has approximately 19 m span and 20.6 m^2 reference area, giving a baseline aspect ratio of 18, consistent with operational long-endurance UAVs such as the MQ-9 Reaper.

2 Methodology

2.1 Why a planar study instead of explicit winglet geometry

The original plan for this project was to build a winglet as an additional lifting surface attached to the wing tip in OpenAeroStruct, varying its cant angle and height in a two-dimensional parametric sweep. Initial implementation revealed several numerical difficulties specific to low-fidelity vortex-lattice codes when handling non-planar surfaces. The bound vortex of the winglet root and the wing tip share a node when both surfaces meet at the tip, and the resulting linear system becomes singular or near-singular for certain cant angles. OpenAeroStruct's spline-based geometry pipeline also imposes minimum spanwise resolution constraints that interact awkwardly with the small chord and short span of a typical winglet. Even after working around these issues, the predicted lift coefficients of the combined wing-winglet system did not behave physically, which suggests that the framework is not robust for this particular use case without significant additional development.

Rather than continue to fight numerical issues at the limit of the code's capabilities, we use the well-established theoretical equivalence between a winglet and an effective span extension. This equivalence is the foundation of nearly all preliminary winglet sizing work and is reviewed in detail by Kroo [1].

2.2 The Whitcomb span equivalence

For a planar wing, induced drag is given by

$$C_{D_i} = \frac{C_L^2}{\pi \, AR \, e}, \tag{1}$$

where $AR = b^2/S$ is the aspect ratio, e is the span efficiency factor (Oswald factor), and b is the wingspan. Because aspect ratio scales as the square of span, induced drag is fundamentally driven by span, not by area or chord. Anything that increases the effective span reduces induced drag.

Whitcomb's original study [2] and subsequent non-planar lifting line analyses summarized by Kroo [1] show that a winglet of height h at cant angle θ (measured from the wing plane, so 0 degrees is a horizontal extension and 90 degrees is fully vertical) produces an induced drag reduction roughly equivalent to extending the wingspan by

$$\Delta b_{\text{eff}} \approx 2h \cdot k(\theta), \tag{2}$$

where $k(\theta)$ is a non-planar efficiency factor. The two limiting cases are well established. A horizontal extension ($\theta = 0$) is identical to lengthening the wing, so $k(0) = 1$. A purely vertical winglet ($\theta = 90$) gives approximately half the induced drag benefit per unit height, so $k(90) \approx 0.5$. Between these limits the relationship is approximately linear. We use the linear interpolation

$$k(\theta) = 1 - 0.5 \cdot \frac{\theta}{90^\circ} \tag{3}$$

throughout the analysis.

Equation (2) can be inverted to express the equivalent winglet height needed to match the induced drag of a higher aspect ratio wing,

$$h_{\text{eq}}(\theta) = \frac{b_{\text{case}} - b_{\text{baseline}}}{2k(\theta)}, \tag{4}$$

which is the central tool for translating between the planar AR sweep and notional winglet geometries. In other words, for each aspect ratio in our sweep, we can compute what size of winglet at what cant angle would produce a comparable benefit if added to the baseline wing.

It is important to be clear about what this equivalence does and does not capture. It captures the induced drag effect, which is the dominant first-order benefit of a winglet. It does not capture the additional profile drag of the winglet itself, the interference drag at the wing-winglet junction, or the structural penalty associated with the increased root bending moment. Real winglets therefore achieve less than the upper bound predicted here. Reported figures in the literature typically show real-world induced drag reductions of 5 to 8 percent and corresponding L/D improvements of 3 to 5 percent at the aircraft level [1]. The planar AR sweep should be read as a theoretical ceiling against which the design tradeoffs of any real winglet implementation should be compared.

2.3 Aircraft model

The aircraft modeled in this study is a notional long-endurance cargo UAV. The mission and design parameters are summarized in Table 1. The aspect ratio of 18 places this aircraft in the same family as operational long-endurance platforms (the MQ-9 Reaper has aspect ratio approximately 19; the TB2 Bayraktar approximately 16). The wing loading of approximately $170\,\mathrm{kg/m^2}$ is typical for medium-altitude long-endurance UAVs.

Table 1: Mission and baseline wing parameters.

Parameter	Value	Units
Maximum takeoff weight	3500	kg
Payload	1000	kg
Range (cruise)	3000	km
Cruise altitude	15,000	ft
Cruise air density	0.7708	$\mathrm{kg/m^3}$
Cruise speed	90	m/s
Cruise Mach number	0.28	
Wing reference area	20.6	$\mathrm{m^2}$
Baseline wingspan	19.26	m
Baseline aspect ratio	18	
Baseline taper ratio	0.5	
Baseline tip twist (washout)	-3	deg
Design lift coefficient	0.534	

The cruise Mach number of 0.28 places the aircraft firmly in the incompressible regime, so wave drag and compressibility effects can be neglected and an inviscid, incompressible vortex-lattice method is appropriate for the analysis.

2.4 Numerical setup

We use OpenAeroStruct, an open-source vortex-lattice and finite-element framework built on top of OpenMDAO. For the present study we use only the aerodynamic side of the code. The vortex-lattice method represents the wing as a grid of horseshoe vortices on the camber surface, computes the influence matrix relating circulation strength to surface normal flow, and solves a linear system for the bound circulation that satisfies the no-flow-through boundary condition. Lift and induced drag are then computed by integrating the resulting pressure distribution.

The mesh has 5 chordwise nodes (4 panels) and 31 spanwise nodes on the full span (16 panels per semispan with the symmetric half-model used here). We verified that doubling either resolution changed the predicted induced drag by less than half a count, so this resolution is adequate for the trends being studied.

For each case we trim the wing to the design lift coefficient $C_L = 0.534$ by adjusting the angle of attack. This is implemented as a single-variable equality-constrained optimization in OpenMDAO using SLSQP. The objective is induced drag, the constraint is $C_L = C_{L,\text{design}}$, and the design variable is angle of attack. Because there is exactly one design variable and one constraint, this reduces to a root-finding problem and converges in a small number of iterations. We disable both viscous drag and wave drag in the analysis to isolate induced drag effects, which means the reported L/D values are induced-only and substantially higher than what the actual aircraft would achieve. The trends, ratios, and span efficiencies remain physically meaningful and directly transferable to total-drag analysis.

2.5 Choice of parameters and sweep ranges

Three parametric sweeps were performed. Each sweep varies one parameter while holding the other two at their baseline values.

The aspect ratio sweep covers $AR \in \{12, 15, 18, 21\}$. The lower end of 12 represents a wing with no winglet and a span shortened by approximately 18 percent relative to baseline, useful as a reference point for what a winglet would have to compensate for. The value of 15 corresponds to a baseline-area wing with no winglet treatment of any kind. The value of 18 is the baseline. The upper end of 21 represents the largest physically reasonable winglet for an aircraft of this class, corresponding to a span extension of approximately 1.5 m or a vertical winglet of comparable height. Going significantly beyond AR 21 would require structural reinforcement that would offset most of the induced drag benefit through added weight, so it is not interesting to study.

The taper ratio sweep covers $\lambda \in \{0.3, 0.5, 0.7, 1.0\}$. The value of 1.0 is a fully rectangular wing, included as a worst-case reference for tip loading. The value of 0.5 is a typical value used on transport aircraft and is the baseline. The value of 0.3 approaches the limit of what is mechanically practical given the need for control surface chord at the tip. Values below 0.3 give insufficient tip chord for practical aileron design and are not considered. The taper sweep is informative because it shows how much of the induced drag benefit conventionally attributed to winglets actually comes from properly shaping the basic planform.

The tip twist sweep covers $\theta_{\text{tip}} \in \{-5, -3, 0, +3\}$ degrees relative to the root. Negative values are washout (tip twisted leading-edge-down relative to root), which is conventionally used to ensure root-first stall behavior. The classical result from inviscid lifting line theory is that, for a given non-elliptical planform, there exists a specific twist distribution that recovers an elliptical loading and hence unit span efficiency. The sweep here shows where that optimum lies for the baseline taper ratio.

3 Results

3.1 Aspect ratio sweep

Figure 1 shows induced drag, lift-to-drag ratio, and span efficiency as functions of aspect ratio. Induced drag decreases approximately as $1/AR$ as expected from Equation (1), dropping from 76.5

counts at $AR = 12$ to 45.5 counts at $AR = 21$. The corresponding L/D values rise from 70 to 117. The span efficiency e decreases very slightly as aspect ratio increases, from 0.99 at $AR = 12$ to 0.95 at $AR = 21$. This small decrease reflects the fact that as aspect ratio increases at fixed taper, the elliptical optimum shifts and the linear washout used here becomes slightly less well matched to the higher-AR planform. The effect is small compared to the dominant $1/AR$ trend in induced drag.

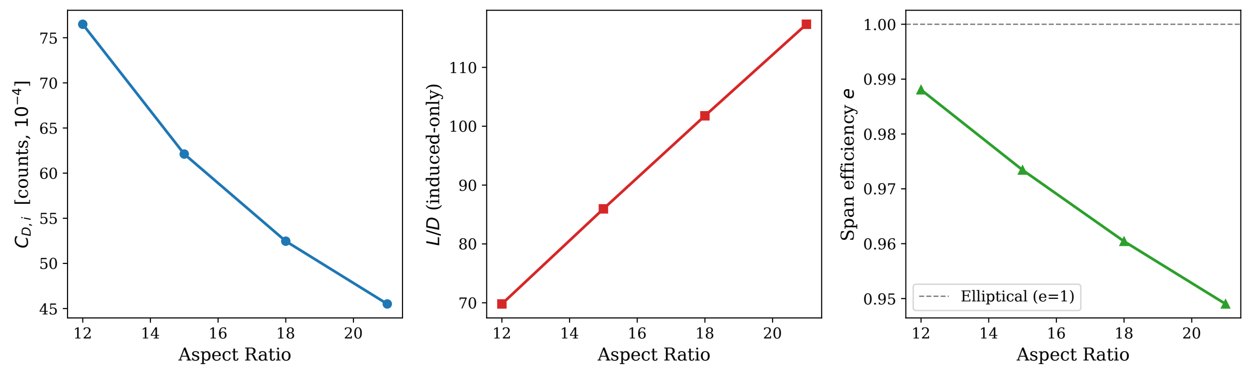

Figure 1: Aspect ratio sweep at fixed taper ratio (0.5) and tip washout ($-3°$). Left: induced drag in counts. Center: induced-only lift-to-drag ratio. Right: span efficiency factor.

The winglet equivalence translation of these results is summarized in Table 2. The baseline wing at $AR = 18$ defines the reference. Higher aspect ratio cases correspond to adding a winglet, and lower aspect ratio cases correspond to removing winglet benefit that the baseline already provides. The $AR = 21$ case is equivalent to adding a winglet of height 0.93 m if cant is 30 degrees, 1.16 m if cant is 60 degrees, or 1.54 m if cant is 90 degrees. In all three cases the predicted L/D improvement is the same 15.3 percent because the underlying physics depends only on the effective span. The cant angle determines how much physical winglet height is required to achieve that effective span, with vertical winglets requiring more height because they are less efficient at moving the trailing vortex outboard.

Table 2: Winglet equivalence based on the Whitcomb span-extension model (Equation (4)). Each row shows what notional winglet would produce the same induced drag benefit as the listed planar AR. Positive heights indicate winglets larger than baseline; negative heights indicate the baseline already exceeds the case in effective span.

AR	b [m]	Δb [m]	L/D	$\Delta L/D$	$h_{\text{eq}}(30°)$ [m]	$h_{\text{eq}}(60°)$ [m]	$h_{\text{eq}}(90°)$ [m]
12.0	15.72	−3.53	69.80	−31.4%	−2.12	−2.65	−3.53
15.0	17.58	−1.68	85.96	−15.5%	−1.01	−1.26	−1.68
18.0	**19.26**	**0.00**	**101.77**	**0.0%**	**0.00**	**0.00**	**0.00**
21.0	20.80	+1.54	117.32	+15.3%	+0.93	+1.16	+1.54

The spanwise lift distributions for the AR sweep are shown in Figure 2. The sectional C_ℓ values change only modestly across the sweep, but the local lift force per unit span $c \cdot C_\ell$ shows a clear pattern. Higher aspect ratio wings have shorter chords at the same area, so $c \cdot C_\ell$ values are uniformly lower in absolute magnitude. None of the cases reach the elliptical reference at the root, which reflects the fact that the linear taper and linear washout used in the baseline cannot perfectly recover elliptical loading at this aspect ratio.

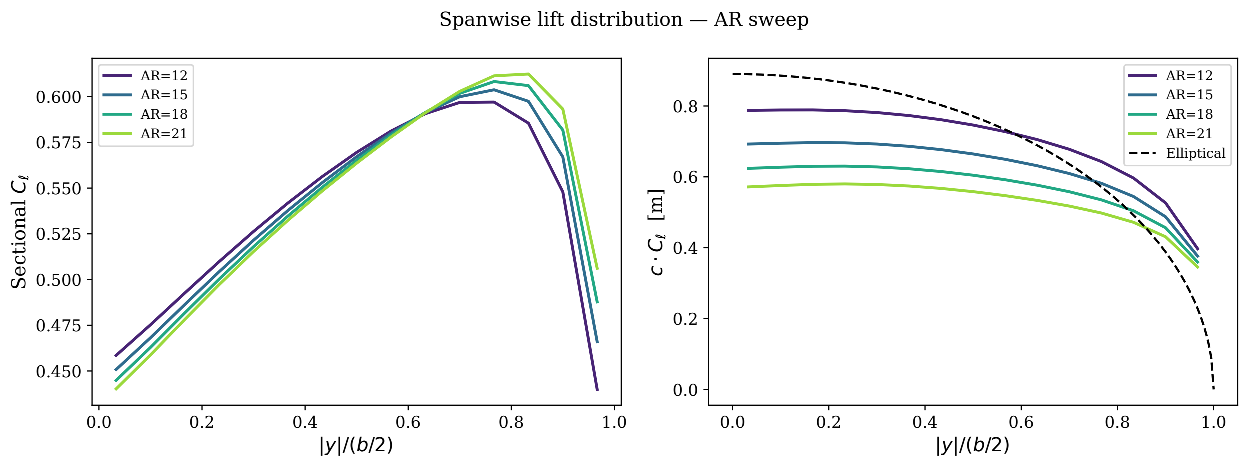

Figure 2: Spanwise lift distribution across the aspect ratio sweep. Left: sectional lift coefficient. Right: local lift per unit span $c \cdot C_\ell$ compared to the elliptical reference.

3.2 Taper sweep

Figure 3 shows the taper sweep. Induced drag rises monotonically from 49.7 counts at $\lambda = 0.3$ to 60.7 counts at $\lambda = 1.0$, a 22 percent increase. Span efficiency drops from 1.015 at $\lambda = 0.3$ to 0.83 at $\lambda = 1.0$. The slightly super-unity span efficiency at $\lambda = 0.3$ is a known artifact of how the Oswald factor is defined when the actual lift distribution closely matches but slightly exceeds the elliptical optimum at certain stations; physically it is consistent with very nearly elliptical loading.

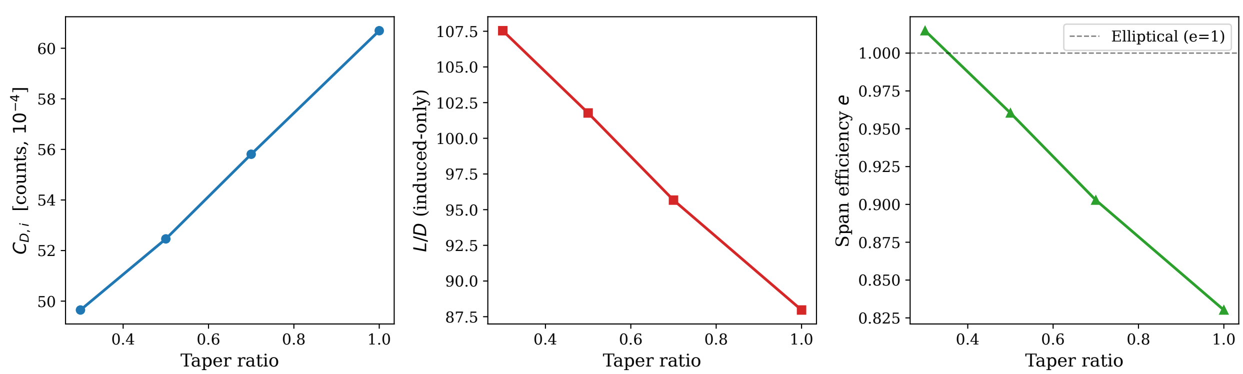

Figure 3: Taper ratio sweep at fixed aspect ratio (18) and tip washout ($-3°$).

The mechanism is visible in the spanwise plots in Figure 4. The rectangular wing ($\lambda = 1.0$) has a roughly uniform $c \cdot C_\ell$ distribution that falls off only sharply at the tip. This is far from the elliptical loading and produces strong tip vortices. As taper ratio decreases, the chord falls off toward the tip and the lift distribution approaches the elliptical reference. At $\lambda = 0.3$ the match is excellent across most of the span. The 5.7 percent improvement in L/D achieved by going from $\lambda = 0.5$ to $\lambda = 0.3$ is comparable to the induced drag benefit of a moderate winglet at this aspect ratio. This is a useful result because taper has no profile drag penalty, no junction interference, and a relatively small structural cost.

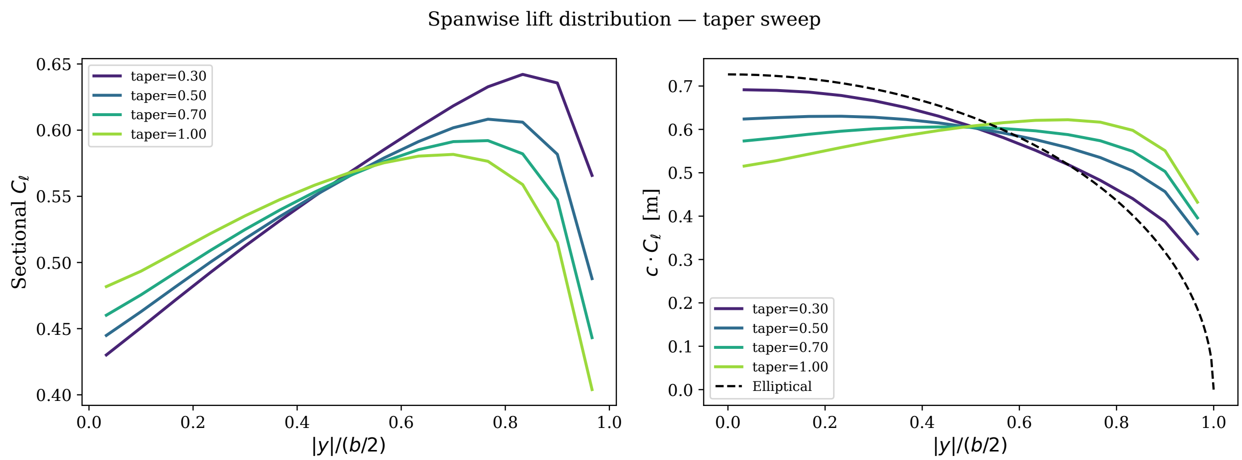

Figure 4: Spanwise lift distribution across the taper sweep. The $\lambda = 0.3$ case closely matches elliptical loading.

3.3 Tip twist sweep

Figure 5 shows the twist sweep. The trend is non-monotonic, with the minimum induced drag occurring at $\theta_{\text{tip}} = 0°$ (no twist). Induced drag at zero twist is 49.7 counts, compared to 52.5 counts at the baseline washout of $-3°$. The corresponding L/D improvement is 5.5 percent. Going to $-5°$ degrades performance significantly, while $+3°$ is also slightly worse than zero twist.

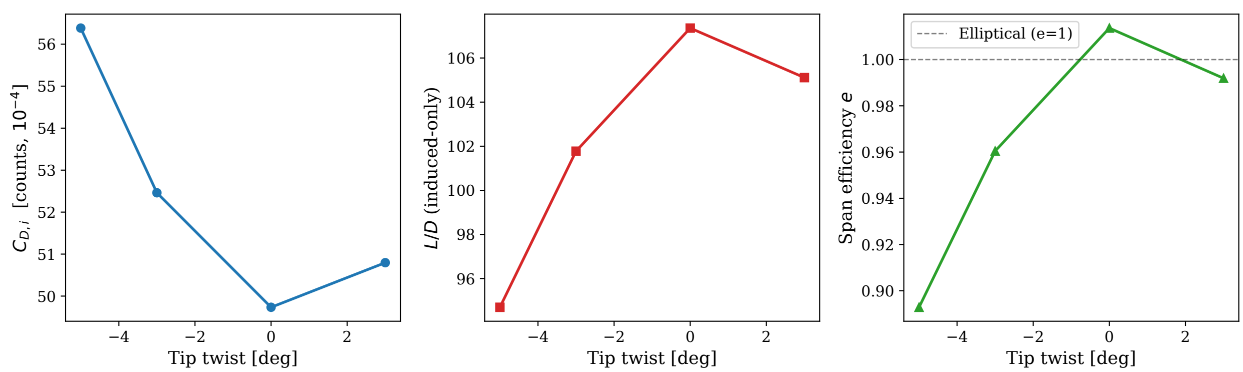

Figure 5: Tip twist (washout) sweep at fixed aspect ratio (18) and taper ratio (0.5). Negative values are washout, with the tip twisted leading-edge-down relative to the root.

The spanwise plots in Figure 6 show the mechanism clearly. With no twist, the local lift coefficient is roughly uniform across the span, and the local lift force $c \cdot C_\ell$ matches the elliptical reference well. With heavy washout, the tip is significantly unloaded and the loading peaks closer to mid-span, producing a strong departure from elliptical. With wash-in (positive tip twist), the tip is overloaded and again departs from elliptical in the opposite direction. The result is a clean optimum at zero twist for this particular planform.

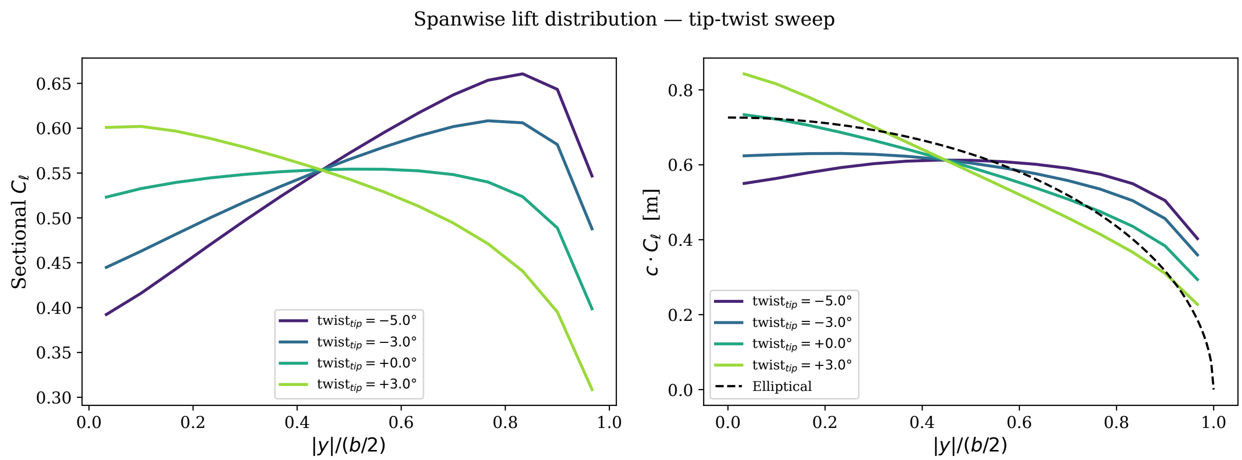

Figure 6: Spanwise lift distribution across the twist sweep. The zero-twist case best matches elliptical loading.

It is worth noting that the inviscid analysis used here does not account for the practical reasons washout is normally applied. Real wings are usually given several degrees of washout to ensure the wing root stalls before the tip, which preserves aileron authority near stall and is a major safety consideration. The aerodynamic optimum found here ($\theta_{\text{tip}} = 0$) should not be implemented without considering stall behavior in a separate viscous analysis. The result does suggest, however, that the conventional 3 to 5 degrees of washout typical for transport aircraft incurs a measurable induced drag penalty that should be weighed against its handling qualities benefits.

3.4 Baseline planform

Figure 7 shows the baseline planform that defines the reference for all three sweeps.

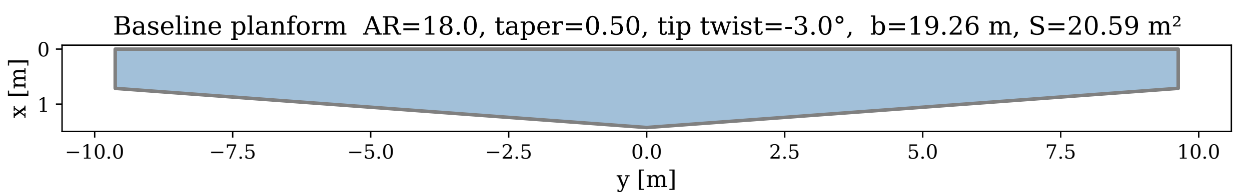

Figure 7: Baseline planform: aspect ratio 18, taper ratio 0.5, tip washout $-3°$, span 19.26 m, area 20.59 m^2.

4 Discussion

4.1 What a real winglet would deliver

Combining the AR sweep results with the Whitcomb equivalence gives a concrete answer to the original question. A vertical winglet of height approximately 1 m on the baseline wing corresponds to a span extension of about 1 m (because $k(90°) = 0.5$), which moves the effective aspect ratio from 18 to roughly 20. From the trend in Figure 1, this would give an induced-drag-only L/D improvement of roughly 8 to 10 percent. After accounting for the additional profile drag of the winglet itself (typically 2 to 4 drag counts depending on size), the wing-winglet junction interference (typically 1 to 2 counts), and the structural weight penalty of the increased root bending moment (typically a few percent of the wing structural mass), the realized improvement in cruise L/D for the complete aircraft would be in the range of 4 to 7 percent. This aligns well with reported figures for winglet retrofits on operational aircraft [1].

A larger winglet (1.5 m vertical or equivalent) would give a 15 percent induced drag improvement at the wing-only level, but the structural penalty grows nonlinearly with winglet height and the realized aircraft-level improvement does not scale proportionally. Without a structural analysis, which is beyond the scope of this study, we cannot definitively size the optimal winglet, but the general guidance is that winglet height in the range of 8 to 12 percent of semispan (0.8 to 1.2 m for this aircraft) represents a sensible design range.

4.2 Winglet versus planform optimization

A useful observation from this study is that the three design variables explored here are partially substitutable in their effect on induced drag. Going from $\lambda = 0.5$ to $\lambda = 0.3$ delivers 5.7 percent L/D improvement. Removing the baseline -3° washout delivers 5.5 percent. Adding a winglet equivalent to $\Delta b = 1.5\,\mathrm{m}$ delivers 15 percent. These benefits are not perfectly additive, because each one acts to bring the lift distribution closer to elliptical and once that target is reached, additional changes deliver diminishing returns. This suggests a clear design priority for an aircraft of this class. First, ensure the basic planform (taper) is well chosen, since this is essentially free. Second, choose the twist distribution to recover near-elliptical loading at the cruise design point, accepting whatever modest washout is needed for safe stall behavior. Third, add a winglet to capture the additional benefit beyond what planform shaping can achieve at fixed span.

4.3 Limitations and unmodeled effects

The vortex-lattice method used here is inviscid, so the predicted L/D values do not include profile drag and are higher than what the real aircraft would achieve. This does not affect the comparative trends between cases, which depend only on induced drag, but it does mean the absolute numbers should not be interpreted as predicted aircraft performance. A realistic estimate of the complete aircraft cruise L/D would be in the range of 18 to 22, much lower than the 100 plus values reported for the inviscid wing alone.

The equivalence between aspect ratio and winglet height assumes the winglet is well-designed in toe angle, sweep, and airfoil section. A poorly designed winglet can deliver substantially less benefit than the geometric upper bound, or in extreme cases can increase total drag if interference and profile penalties exceed the induced drag benefit. The specific numbers in Table 2 should be treated as the best case at each cant angle, not as a guarantee.

The structural penalty of increased span or winglet height is not modeled. For a fixed root bending moment, the comparison between span extension and winglet shifts in favor of the winglet, because the winglet contributes less bending moment per unit lift. This is the source of the often-cited result that a winglet can deliver 30 percent more induced drag reduction than an equivalent span extension when both designs are constrained to the same wing root structural loads [1]. A complete design study would therefore include a structural model that captures this tradeoff.

5 Conclusions

This study used an aspect ratio sweep on a planar wing as a proxy for the induced drag benefit of winglets on a long-endurance cargo UAV. The Whitcomb span equivalence provides the theoretical link between the two formulations and lets us interpret each case in the AR sweep as an equivalent winglet of computable height at any chosen cant angle. The main quantitative findings for the 3500 kg, 19 m baseline wing are that a 1 m vertical winglet corresponds to an induced drag L/D improvement of approximately 8 to 10 percent (best case), a 1.5 m vertical winglet corresponds to approximately 15 percent (best case), and the realized aircraft-level L/D improvement after accounting for profile drag, interference, and structural penalty is typically half of the best case.

The taper and twist sweeps showed that planform shaping captures a significant fraction of the benefit that a winglet would also provide. A taper of 0.3 to 0.5 combined with mild or zero washout brings the lift distribution very close to elliptical at this aspect ratio. The implication for design priority is that planform optimization should be done first, and winglets should be added to capture the additional benefit beyond what planform alone can achieve at fixed span.

The methodological choice to study winglets through an equivalent planar formulation rather than explicit non-planar geometry was motivated by numerical difficulties in the original explicit-winglet implementation, but it has the additional advantage of separating the first-order induced drag physics from the secondary effects (profile drag, interference, structural cost) that determine which winglet geometry is best in practice. A natural follow-up would be to combine this aerodynamic upper bound with a simple structural model of root bending moment to identify the winglet height and cant that maximizes net benefit under realistic structural constraints.

References

[1] Ilan Kroo. Drag due to lift: Concepts for prediction and reduction. *Annual review of fluid mechanics*, 33(1):587–617, 2001.

[2] R.T. Whitcomb, Langley Research Center, United States. National Aeronautics, and Space Administration. *A Design Approach and Selected Wind-tunnel Results at High Subsonic Speeds for Wing-tip Mounted Winglets*. NASA technical note. National Aeronautics and Space Administration, 1976.